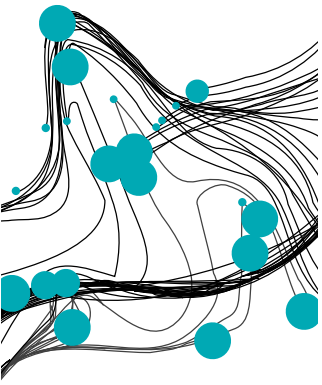

RAM ROBOTICS AND MECHATRONICS

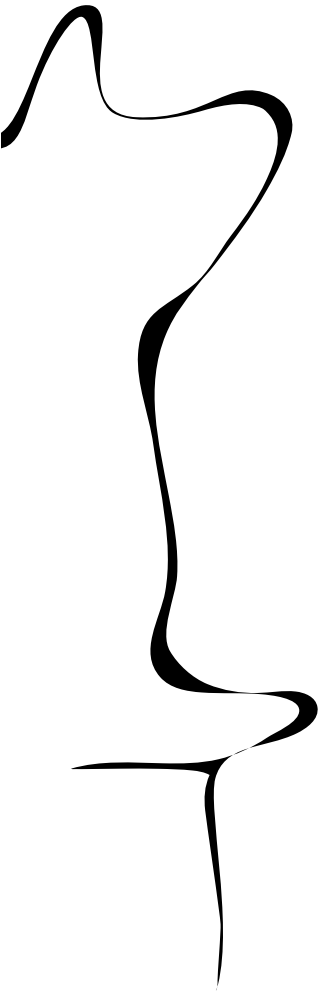

Acousto-Mechanical Imaging with 3D Printed Ultrasound Probe Extension

N. (Nart) Pistorius

BSC ASSIGNMENT

Committee:
prof. dr. ir. G.J.M. Krijnen
M.K. Welleweerd, MSc
dr. ir. A.P. Berkhoff

July 2020

025RaM2020
Robotics and Mechatronics
EEMCS
University of Twente
P.O. Box 217
7500 AE Enschede
The Netherlands

UNIVERSITY OF TWENTE. | TECHMED CENTRE UNIVERSITY OF TWENTE. | DIGITAL SOCIETY INSTITUTE

Abstract

Ultrasonic imaging and mechanical imaging are techniques for medical diagnoses for cancer and biopsy assistance in human breast tissue. Combining the two techniques could have a superior performance compared to both techniques alone. The implementation idea is to have a 3D printable structure in between an ultrasound probe and human tissue. Which deforms when the ultrasound probe is pressed to the tissue. For hard inclusions in the breast the structure should deform differently. The structure is box shaped and fluid filled. It is fluid filled because fluid should preserve the ultrasonic imaging resolution. The effective stiffness of the structure should be in between the stiffness of lesion and normal tissue. The effective stiffness can be approximated for small strain (up to 1%) by the equation for axial compression in 2D finite element analysis. For larger strains elongation of the beam should be considered.

Keywords: Acoustic-Mechanical Imaging (AMI), Effective stiffness of fluid filled deformable container.

Contents

1 Introduction

1.1 Context

About 1 out of 7 women are diagnosed with breast cancer during their lifetime in the Netherlands. There's a good chance of recovery if it's detected at an early stage (Wauben, 2018). Therefore it is vital to identify changes in the breast tissue (lesions) in the earliest phase possible.

The most used identification method is mammography. A mammogram is a low-dose X-ray picture of a breast. An image is often not sufficient to determine the existence of benign or malignant disease with certainty. If abnormalities are found further diagnostic studies may be recommended like magnetic resonance imaging (MRI), ultra-sound (US) or biopsy.

MRI is used to help determine the extend of the breast cancer, to help measure the size of the lesion and to check for other tumors in the breast. Although MRI can find some cancers not seen on a mammogram, it's also more likely to find things that turn out not to be cancer (called a false positive) (Tzias et al., 2018) i.e. the specificity is not high. This can result in a woman getting biopsies that end up not being needed.

A biopsy is executed if the nature of the lesion is unknown. During a biopsy, a small piece of lesion is removed such that it can be analysed. Biopsy can be guided with MRI as well as with US. MRI has a higher resolution than US leading to better guidance, but MRI is not displaying real time and US is.

Ultrasound is used in most cases for further diagnoses of found abnormalities. The ultrasonic image displays various tissue structures such as fat, breast tissue, bone and cysts. Abnormalities smaller than 5 mm are not always detected (Tzias et al., 2018). Ultrasound is user dependent, meaning that the reproducibility of the diagnosis is inferior.

Another relative new diagnostic tool is mechanical imaging (MI), it is based on reconstruction of tissue structure and viscoelastic properties using mechanical sensors. Cancerous tissue is stiffer than normal breast tissue (Krouskop et al., 1998). Hard inclusions can be detected by the stress distribution at the skin interface when the breast tissue is compressed. This could be used for diagnosis but also for biopsy guidance.

The combination of ultrasonic imaging and mechanical imaging, referred to as acousto-mechanical imaging (AMI), could have a diagnostic and biopsy guidance performance superior to both imaging modalities alone.

The combination could be realized by adding a structure between the ultrasonic probe and the tissue (Fig. 1.1). The structure should deform as result of the probe pressed to the tissue. The deformation of the structure conveys the information about the tissue structure and properties like stiffness. The deformation of the structure could be determined with the US scan, by looking at the envelope of the interface between the structure and the tissue. The structure should not cause poor performance of the US scan. Meaning that the structure should be transparent for US. For this reason the structure will be fluid filled. What the optimal effective stiffness should be in order to detect lesions and how to achieve an optimal acoustic impedance match are also relevant questions but beyond the scope of this thesis.

1.2 Thesis Scope

The focus of this thesis is on modeling the deformation of a fluid filled container. The model is validated with Ansys simulations. The main research questions are:

- How to model a fluid filled deformable structure between an ultrasound probe and tissue?

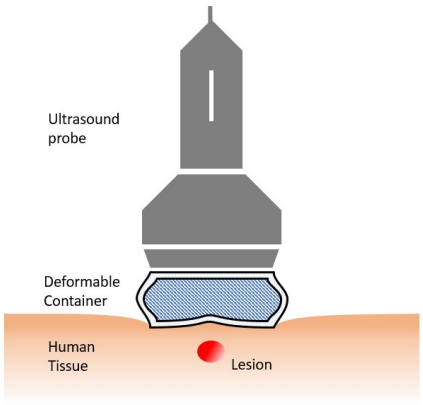

Figure 1.1: Acousto-mechanical imaging implementation with a fluid filled container in between the ultrasound probe and human tissue

- What is the stiffness of a fluid filled deformable structure?
- Which parameters influence the stiffness of fluid filled structure?

1.3 Thesis Outline

In chapter 1 background information is presented as stepping stones for the later chapters. Followed by chapter 3 which is about the mechanical analysis of a fluid filled deformable container. The simulation method for validation of the analysis is explained in chapter 4. The results are presented in chapter 5 and discussed in chapter 6. The thesis is concluded in chapter 7.

2 Background Information

This chapter will cover background information. First the background for fluid filled structures is given in the context of the properties of ultrasonic imaging. Secondly important properties of mechanical imaging are described. Thirdly, hyperelastic material properties are defined.

2.1 Ultrasonic Imaging

The structure in between the US probe and the tissue should be as acoustically transparent as possible (Fig. 1.1). This implies that the acoustic impedance of the structure should be as close to the impedance of the tissue. In Tab. 2.1 some impedance values are shown.

The acoustic impedance is given by the density [$\mathrm{kg\,m^{-3}}$] of the material times the speed of sound [$\mathrm{m\,s^{-1}}$] in the material (Garett, 2017).

$$Z = \rho v \tag{2.1}$$

Another important factor for maximal transmission through the structure is the absorption coefficient. It is the amount of absorption per unit of length at a certain frequency. The absorption of the structure should be as low as possible.

Material	**Density** ρ [$\mathrm{kg\,m^{-3}}$]	**Speed** c [$\mathrm{m\,s^{-1}}$]	**Impedance** Z [$\mathrm{M\,kg\,m^{-1}\,s^{-2}}$]	**Absorption** α [$\mathrm{dB\,cm^{-1}}$ at 1MHz]
Air	0.0012	330	0.0004	1.38
Water at 20° C	997	1480	1.48	0.0022
Water at 37° C	990	1530	1.51	0.003
Fat	920	1450	1.35	0.63
Soft tissue	1100	1540	1.69	0.5 - 1
US gel	1021 - 1053	1546 - 1595	1.58 - 1.68	0.08 - 0.14
Rubber-like material	900-1300	1300-1700	1.17-2.21	0.7 - 10

Table 2.1: Acoustic impedance values for various of materials (Wolbarst, 1993), (Zhang, 2013)

The impedance of water at 22°C is 12% smaller than the impedance of the tissue. The impedance of the US gel can be the same as the impedance of the tissue. But water has a lower absorption coefficient. Rubber-like materials have a higher absorption coefficient. When the deformable structure is made from rubber like material, the accuracy of the ultrasonic scan decreases. Thus for this reason the deformable structure is filled with liquid material.

The force applied by the user on the probe is typically 0 N to 8 N (Burcher et al., 2005). This user can be a human as well as a robot.

The probe head is in contact with the skin. Most probes have a rectangular head where one end is way longer compared with the other. The length of the the long end is referred to as the footprint of the probe. This varies for different types of probes with different types of applications. Probes designed for breast scanning or guidance of breast biopsy have a footprint of around 6.8 mm (Siemens, 2004).

2.2 Mechanical Imaging

The breast of a woman consists of several types of tissue. Each type of tissue has its own mechanical properties. One of the mechanical properties is the stiffness, which most closely corresponds to the physical parameter called the Young's modulus. Cancerous tissue happens to be stiffer than normal tissue (Krouskop et al., 1998). This is what is used during manual palpa-

tion. The human finger acts as a pressure sensor and detects stiffer lumps present under the skin.

The tissue types are assumed to be linear elastic, which is valid for small strains. For linear elastic materials the stress strain curve of the material is linear (Eq. 2.2).

$$E = \frac{\sigma}{\epsilon} \tag{2.2}$$

Where E is the Young's modulus [Pa], σ the stress [Pa] and ϵ is the strain which is dimensionless.

Breast tissue type	**Young's Modulus (kPa)**	
	5% precompression	20% precompression
Normal fat	18 ± 7	20 ± 5
Normal glandular tissue	28 ± 14	58 ± 15
Fibrous tissue	96 ± 34	218 ± 87
Ductal carcinoma in situ	22 ± 8	291 ± 67
Invasive and infiltrating ductal carcinoma	106 ± 32	558 ± 180

Table 2.2: Tissue elastic modulus for different breast tissue types for a 5% and 20% precompression and loading frequency of 0 1Hz (Krouskop et al., 1998)

If the effective stiffness of the structure would be larger than the stiffness of inclusion, then the tissue and inclusion would be pressed and the sensing structure would not deform. If the effective stiffness of the structure would be much smaller than the stiffness of normal tissue, the structure would just take the shape of the tissue. Thus the effective stiffness of the structure should be in between the normal tissue and cancerous tissue stiffness's.

2.3 Material

The container will be made from a rubber like material. The stress strain relation of rubber like material is referred to as hyperelastic. The stress strain curve is typically S-shaped. Hyperelastic materials can sustain large elastic (recoverable) deformations and are almost incompressible. The stress strain relationship exhibits strong non-linearity. Usually, under tension, the material softens and then hardens, and the material hardens sharply when it is compressed (Fig. 2.1) (Baranowski et al., 2013).

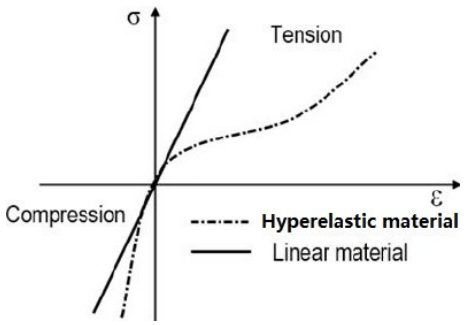

Figure 2.1: Stress strain relation of hyperelastic material (Baranowski et al., 2013)

Concluding this chapter, water like fluid have more or less the same impedance as human tissue and is therefore used inside the container. The stiffness of structure should be in between the stiffness of normal and cancerous breast tissue.

3 Analysis of Fluid Filled Deformable Container

This chapter is about the mechanical model of the container filled with fluid. First an analysis is given for only lateral load. In the second part of this chapter also axial loading is considered. First axial compression and next axial tension.

3.1 Only Lateral Loading

A logical shape of the container is a cuboid (i.e. box shaped), since the probe face is rectangular. This cuboid can be represented in 2D as a rectangle shown in 3.1. With this 2D representation the system is considered as infinitely long in z-direction, i.e. there is no change with z-direction. All dimensions and forces are per unit length in z-direction.

The top of the box is assumed to be rigid and thus not to bend, because the US probe is attached here (Fig. 1.1). The bottom is pressed to the tissue and should bend if there are inclusions in the tissue. But since the structure should be stiffer than the normal tissue, it can be considered rigid as well if pressed onto normal breast tissue. This leaves us with 2 sides which can deform and can be modeled as 2 beams. The pressure of the fluid inside will rise if the box is pressed and this fluid pressure causes the sides to bend. Beside the fluid pressure on the sides there is also axial loading on the beams (Fig. 3.2). For now only pure bending of the sides will be considered, thus the axial force P (Fig. 3.2) is zero. Furthermore, it is assumed that the beams have a uniform Young's modulus and constant thickness.

The fluid inside the container can be modeled as incompressible. Since the bulk modulus of water is about 2.2 GPa Thus the displaced areas at the side walls should be equal to the displaced area at the bottom (Fig. 3.1). This is written down in equation 3.1.

$$2A_{\text{side}} = Ldh \tag{3.1}$$

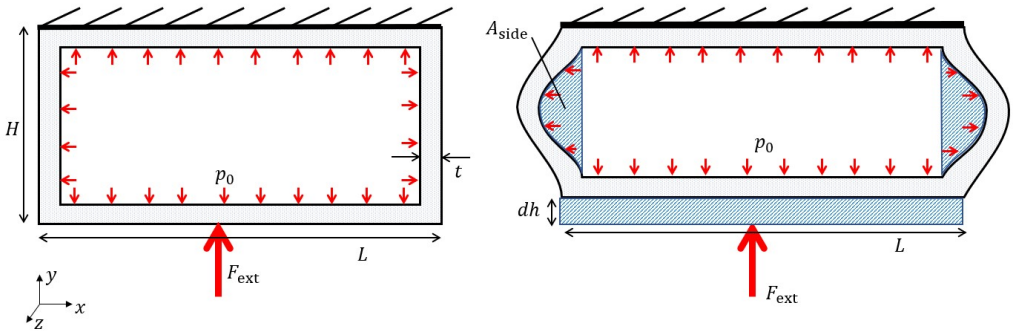

Figure 3.1: Fluid filled container with hard bottom and top, left is the structure in undeformed state and right deformed with bend sides

For the deformation of a beam under lateral loading Eq. 3.2 (Beer, 2012) applies. The situation is illustrated in Fig. 3.2.

$$EI\frac{d^4u}{dy^4} = -q(y) \tag{3.2}$$

Where u is the displacement of the bend beam [m], E is the Young's modulus of the material [Pa], I is the second moment of inertia of the geometry [m^3] and $q(y)$ is the lateral load [$N\,m^{-1}$].

This lateral load acting on the beam can be considered uniform if gravity is neglected. Gravity can be neglected because the pressure due to the gravity acting on water will be small compared

to the pressure applied by the probe. If the box has a length of 7 cm long, a width of 3 cm and a height of 3 cm the pressure difference between the top and bottom is about 300 Pa due to gravity Eq. 3.3, while the p_0 is 5 kPa (8 N over 3 cm by 7 cm).

$$p = p_0 + \rho g h \tag{3.3}$$

The pressure applied by the probe (F_{ext}/L) should be equal to the pressure of the fluid.

$$q(y) = p_0 = \frac{F_{\text{ext}}}{L} \tag{3.4}$$

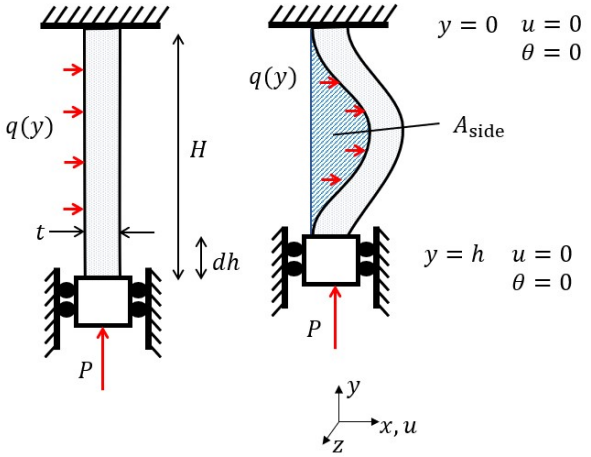

Figure 3.2: Bending of side wall where the deflection and the angle is zero at the boundaries for $y = 0$ and $y = h = H - dh$ and where q is the lateral load and P the axial

Integrating Eq. 3.2 four times and inserting Eq. 3.4 results in:

$$EI\frac{d^4u}{dy^4} = -p_0 \tag{3.5}$$

$$EIu = -\frac{1}{24}p_0y^4 + \frac{1}{6}C_1y^3 + \frac{1}{2}C_2y^2 + C_3y + C_4 \tag{3.6}$$

The bottom and top of the beam are fixed to the bottom and top of the box. Let call the beam the part where the lateral loading is acting upon. The part above and below the beam can also deform. But this corner bending is neglected for this analysis. Thus the connection is considered rigid and therefore the angle of the beam at the bottom and top should be constant zero degree with respect to the y axis. Considering the bottom and top rigid, the beam should not be able to move in x direction at the connection points.Thus the boundary conditions (BC) are:

$$\text{at} \quad y = 0 \qquad \Longrightarrow \quad u = 0 \quad \text{and} \quad \theta = \frac{du}{dy} = 0 \tag{3.7a}$$

$$\text{at} \quad y = H - dh \quad \Longrightarrow \quad u = 0, \quad \text{and} \quad \theta = \frac{du}{dy} = 0 \tag{3.7b}$$

Solving for integration constants lead to the deflection, Eq. 3.8. See appendix A for further elaboration.

$$u = \frac{p_0}{24EI}\left(-y^4 + 2(H-dh)^3 - (H-dh)^2y^2\right) \tag{3.8}$$

The area A_{side} is the integral under the curve u from zero to the roller BC, which is located at $H - dh$.

$$A_{\text{side}} = \int_{y=0}^{y=H-dh} u(y)\mathrm{d}y \tag{3.9}$$

$$= \int_{y=0}^{y=H-dh} \frac{1}{EI}\left(-\frac{p_0}{24}y^4 + \frac{p_0(H-dh)}{12}y^3 - \frac{p_0(H-dh)^2}{24}y^2\right)\mathrm{d}y \tag{3.10}$$

$$= \frac{p_0}{EI}\left[-\frac{1}{120}y^5 + \frac{(H-dh)}{48}y^4 - \frac{(H-dh)^2}{72}y^3\right]_0^{H-dh} \tag{3.11}$$

$$= -\frac{p_0(H-dh)^5}{720EI} \tag{3.12}$$

Filling this in Eq. 3.1, results in:

$$Ldh = 2\frac{p_0(H-dh)^5}{720EI} \tag{3.13}$$

The second moment of inertia [m^3] is given by the inertia of the beam per meter, because it is a 2D analysis.

$$I = \int_{-t/2}^{t/2} x^2 dx = \left[\frac{x^3}{3}\right]_{-t/2}^{t/2} = \frac{t^3}{12} \tag{3.14}$$

Rewriting Eq. 3.13 using Eq.3.4 and 3.14.

$$F_{\text{ext}} = \frac{30Et^3L^2}{(H-dh)^5}dh \tag{3.15}$$

If the delta height dh tends to go to the height H then the external force tends to infinity.

Equation 3.15 is plotted in Fig. 3.3.

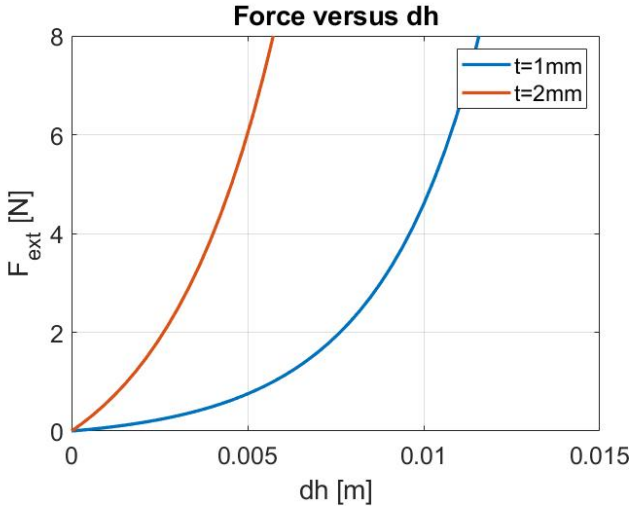

Figure 3.3: Graph F_{ext} versus dh of Eq. 3.15 for H=3 cm, L=7 cm, E=10 kPa

For small dh ($dh << H$) Eq. 3.15 can be simplified to the following equation.

$$F_{\text{ext}} = \frac{30Et^3L^2}{H^5}dh \tag{3.16}$$

3.2 Axial Compression and Lateral Loading

If the axial force P in Fig. 3.2 is not zero, then the deformation of the beam is given by Eq. 3.17 (Timoshenko, 1989). Beams subjected to axial compression and simultaneous supporting lateral loads are known as beam-columns.

$$EI\frac{d^4u}{dy^4} + P\frac{d^2u}{dy^2} = q(y) \tag{3.17}$$

The solution to this differential equation is given by the homogeneous plus the particular solution.

$$u(y) = C_1\sin(ky) + C_2\cos(ky) + C_3y + C_4 + \frac{qy^2}{2P} \tag{3.18}$$

Where $k^2 = P/EI$ and C_1 to C_4 are constants of integration that must be evaluated at the boundary conditions. The boundary conditions are the same as for pure bending Eq. 3.7. See appendix A for further elaboration.

$$C_1 = -\frac{C_3}{k} \tag{3.19a}$$

$$C_2 = \frac{2q(H-dh)\sin(k(H-dh)) + 2q(H-dh)^2k - q(H-dh)^2k\{1-\cos(k(H-dh))\}}{2Pk\{2\cos(k(H-dh)) + k(H-dh)\sin(k(H-dh)) - 2\}} \tag{3.19b}$$

$$C_3 = \frac{C_2kP\sin(k(H-dh)) - q(H-dh)}{P\{1-\cos(k(H-dh))\}} \tag{3.19c}$$

$$C_4 = -C_2 \tag{3.19d}$$

The total external force can be divided into a part which causes the axial load and the lateral load, i.e. a part which compresses the beams and a part that causes the rise in pressure in the fluid. Let α be a constant between 0 and 1 to divide the external load. For α equal to 1 the solution should be the same as for the previous analysis. For this analysis half the system is analysed and after wards the external force is multiplied by 2. The line over which the external force is applied is halved.

$$q = \frac{F_{\text{ext}}\alpha}{L/2} \tag{3.20}$$

$$P = F_{\text{ext}}(1-\alpha) \tag{3.21}$$

The area under the curve of Eq. 3.18 from zero to $H-dh$ is given the following equation. This is the same integral approach as in the pure bending model Eq. 3.9. But now the A_{side} should be equal to $Ldh/2$ because of half the system analysis.

$$A_{\text{side}} = -\frac{2C_1}{k}\cos(k(H-dh)) + \frac{2C_2}{k}\sin(k(H-dh)) + \frac{2C_3}{2}(H-dh)^2 + 2C_4(H-dh) + \frac{2q}{6P}(H-dh)^3 + \frac{2C_1}{k} = \frac{L}{2}dh \tag{3.22}$$

This equation is numerically solved by finding the intersection point of the middle part and right hand side of the equation. In other words the point (dh) for which the areas are equal for the set force is found. The solution is graphed in Fig. 3.4.

The solution is existing until the critical force P_{crit}. Because the deflection of the beam (Eq. 3.18 with the constants of Eq. 3.19) tends to infinity at for this critical force. With the deflection tending to infinity the area under the curve also is. Thus yielding no physical solution for forces greater than this force. This is the critical force for half the system, for the full system the force should be doubled. This equation is also know as Euler formula and for different end conditions of the beam the effective length (K) changes. For a fixed-fixed beam the effective length factor is 1/2 (Beer, 2012).

$$P_{\text{crit}} = \frac{\pi^2 EI}{(KH)^2} \tag{3.23}$$

This point for which the deflection goes to infinity is only dependent on the axial loading, not on the lateral loading.

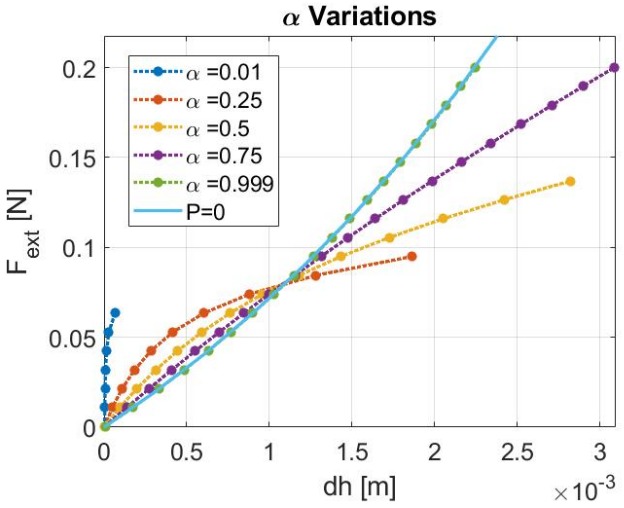

Figure 3.4: Graph of Eq. 3.22 for variations of α and Eq. 3.15 (solid line) with H=3 cm, L=7 cm, E=10 kPa, t=1 mm and P_{crit}=0.0732 N

For α equal to almost 1 the solution of Eq. 3.22 is similar to the solution of the previous section which is as expected (Fig. 3.4). For a smaller α the curve tends to be steeper for the beginning and flattens out after some point. The steeper beginning is caused of less to almost none for $\alpha = 0.01$ external force going to the lateral load. The curves tends to flatten out because of the approaching critical load.

3.3 Axial Tension and Lateral Loading

In the previous section axial compression is considered. But this might only be valid for small displacements. With axial compression the sides are pushed, i.e. compressed in y-direction. But at some point the sides start pulling on the top and bottom because the sides are pushed out and start to stretch instead of compress. With axial tension the same Eq. 3.17 applies as in the case of compression. But the force P in Eq. 3.21 is now negative. For $\alpha > 1$ the force P becomes negative. The external force is now divided into a positive and negative part, which sum up to the external force. The negative force at the sides is caused by elongation of the beam. For large external forces the water is pushed out against the walls hard enough such that the beam starts elongating and causing the negative force. This negative force is modeled here.

In Fig. 3.5 Eq. 3.22 is plotted for variations of α. For α between zero and one the beam-columns are under compression and for α between one and two the beam-columns are under tension. But now 'beam-columns' is (for α between 1 and 2) not the right word anymore since columns

can collapse, in other words the the deflection goes to infinity for certain force. For α between 1 and 2 it can not collapse. So we should call it beams again.

For α=0.9 (compression) the structure is less stiff than only lateral loading and for α=1.1 (tension) the structure is stiffer compared to only lateral loading.

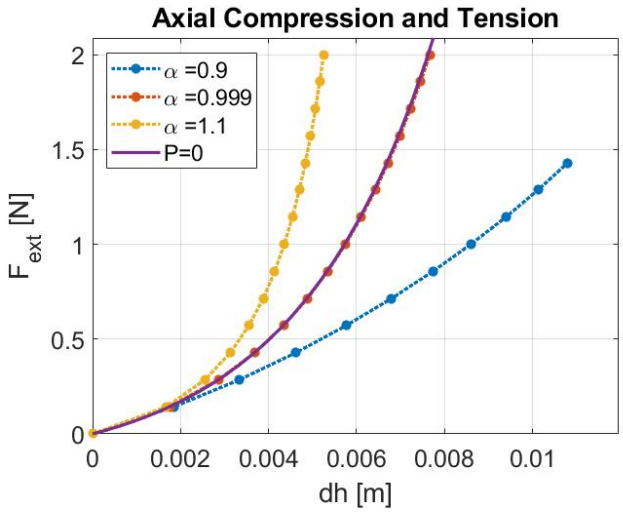

Figure 3.5: Graph of Eq. 3.22 for variations of α, α=0.9 implicates compression and α=1.1 tension and the solid line is Eq. 3.15 with H=3 cm, L=7 cm, E=10 kPa and t=1 mm

Concluding this chapter, the stiffness of the structure is modeled for three different loading conditions. For all models the solution is increasing non-linearly for larger strains. The lateral and axial loading solution includes the only lateral solution.

4 Simulation

This chapter will cover 2D simulations in Ansys for comparison with the analysis done in the previous chapter. First the simulation setup will be explained. Followed by setup and explanation for simulation without corners. Lastly the simulation without fluid inside the container is clarified.

4.1 2D simulation

The simulation will be done in 2D in Ansys APDL (ANSYS, Inc., 2020). The walls of the container are set as a 4 nodal structural solid element type (PLANE182) with linear elastic properties. The 2D simulation will be done under the assumption of plane stress. Plane stress is applicable if the thickness of the structure is small relative to the other dimensions. Which is the case because the walls are relative thin compared to the length and the width.

The water inside the container is assigned with a specific hydrostatic fluid element, called HSFLD241. This element permits Ansys to include a contained fluid inside a shell or solid model of a container, in order to capture the effect of fluid pressure and fluid mass on linear, modal dynamic, plus nonlinear static and transient dynamic models. "Contained" means they do not include a free surface, and so are not used to model "sloshing" movements of a liquid with a free surface. The pressure in the fluid is assumed to be uniform, thus the gravity will not be taken into consideration. This element type is applied by letting the inner sides of the container all share the same node in the middle (Fig. C.1). The nodes at the inner side of the container plus the node in the middle share the same pressure.

The displacement of the bottom and top of are set equal to zero in x-direction. The bottom displacement in y-direction is set to be zero. The load is set as a displacement in y-direction at the top. Because applying a pressure results in bending of the top, which is not ideal for comparison with the analysis. Thus the top is displaced and the integrated reaction pressure gives the force required to displace the top. All the reaction forces at the nodes positioned at the top are summed up to give the external force.

For the simulation the following parameters are used unless noted otherwise.

Parameter	**Name**	**Value**
Height	H	3 cm
Length	L	7 cm
Young's Modulus	E	10 kPa
Thickness	t	1 mm

Table 4.1: Simulation parameters

4.2 2D Simulation without Corners

In the analysis (Chap. 3) the ends of sides (BC) are not to move in x-direction and not have an angle. In the previous simulation both BC's can be violated. Thus to find out about the influence of the corners this simulation is done and to analyse the reaction forces acting on the sides and the top. The reaction forces on the top (F_{top}) can now only be caused by the pressure of the fluid. The relation between the reaction forces can give insight on the value for α.

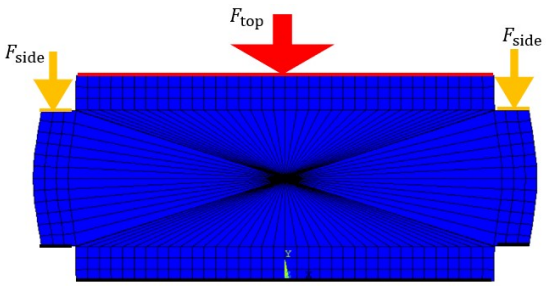

Figure 4.1: No corners with large thickness for the illustration

4.3 2D Simulation without Fluid

Lastly a simulation is done without water inside the container. For this setup there are basically 2 beams in parallel that would deform according to Eq. 4.1 until the critical load is reached (Eq. 3.23). In this case that is 0.0732 N.

$$dh = \frac{F_{ext} \cdot H}{2 \cdot t \cdot E} \tag{4.1}$$

Concluding this chapter, the method of simulation with Ansys is covered. Plane stress is assumed for the container and the fluid is modeled with a incompressible fluid element. Simulation will run for the structure, the structure without corners and the structure without fluid inside.

5 Results

5.1 Simulation vs Analysis P=0

In Fig. 5.1 the simulation curve for all thicknesses fluctuates over the analysis curve (only lateral loading). This is also the case for Fig. 5.2 for both Young's moduli. The simulation curve has in all cases a dip, which can be described by a phenomenon called snap-through buckling. Which is a limited equilibrium instability in the system. Under certain loading the system may pass from an equilibrium state to a non-adjacent equilibrium configuration. The force at the peak is the critical force.

For thicker walls of the structure the stiffness is larger as can be seen from Fig. 5.1. The location of the dip (or local maximum) is dependent on the thickness. For thicker walls the dip is found at larger F_{ext}.

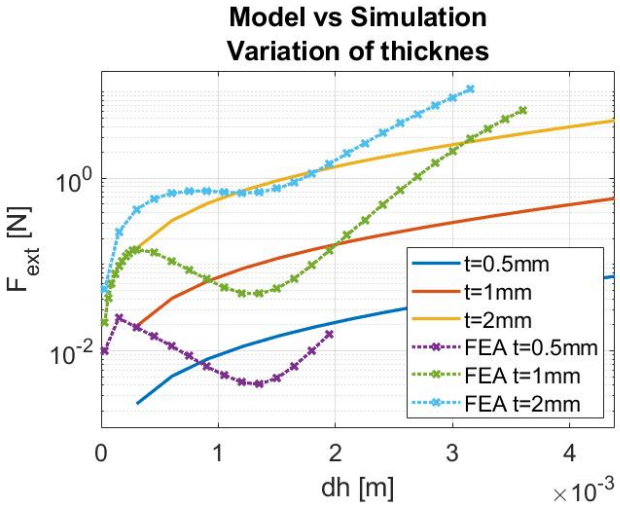

Figure 5.1: External force on logscale versus dh for simulation (dashed lines) and analysis of Eq. 3.15 (solid lines) for 3 thickness values 0.5 mm, 1 mm and 2 mm

For a larger young's modulus of the material the structure is stiffer (see Fig. 5.2).

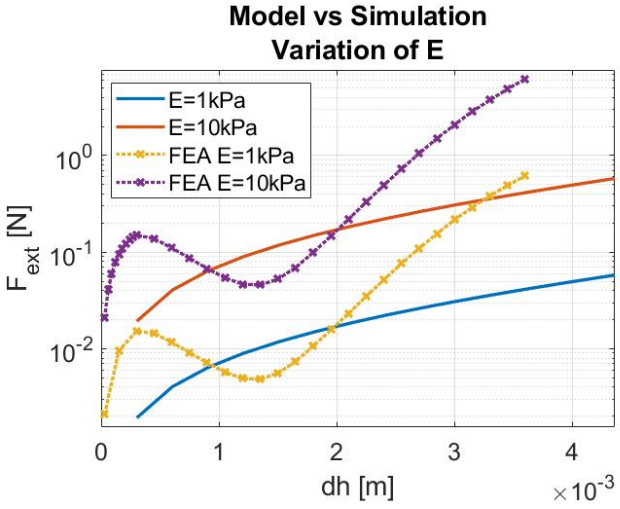

Figure 5.2: External force on logscale versus dh for simulation (dashed lines) and model of Eq. 3.15 (solid lines) for 2 Young's modulus values 1 kPa and 10 kPa

5.2 Simulation with corners vs simulation without Corners

The simulation with the corners, blue dotted line in Fig. 5.3, and simulation without corners, red line, start to deviate notably for a dh of 2 mm. Thus the effect of the corners in the simulation for thickness 1 mm is minimal for structural strain (dh/H) up to 6% (dh=2 mm in Fig. 5.3). For larger structure strain the force required for the same strain is higher for the simulation without corner than with.

For forces under the critical load the forces on top of the container are approximately 5% of the forces on the sides. Thus for small strains of the structure the dominant force is is on the side walls. Where for larger strains the the forces on the top pressing down on the fluid are larger. For example for dh =3 mm (strain of 10%) the forces on the beam-columns are approximately 15% of the force total force.

Another observation that the forces on the top of the box first are negative and increases and becomes positive after a certain displacement. The forces acting on the beam-columns top are positive for the small displacements but for larger values the forces become negative.

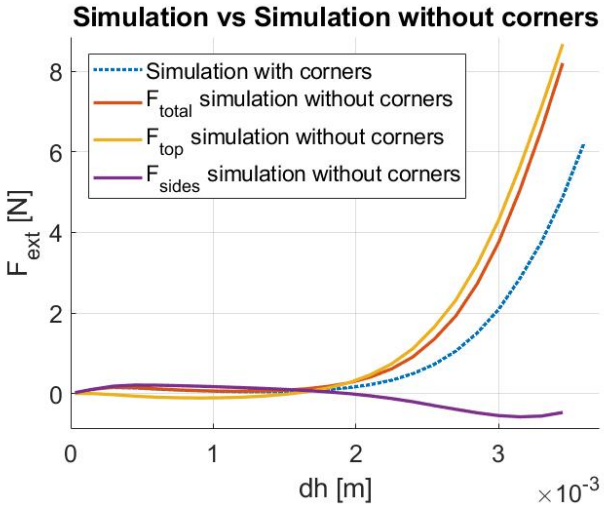

Figure 5.3: Reaction forces for different section of the structure the top and side force are defined in Fig. 4.1

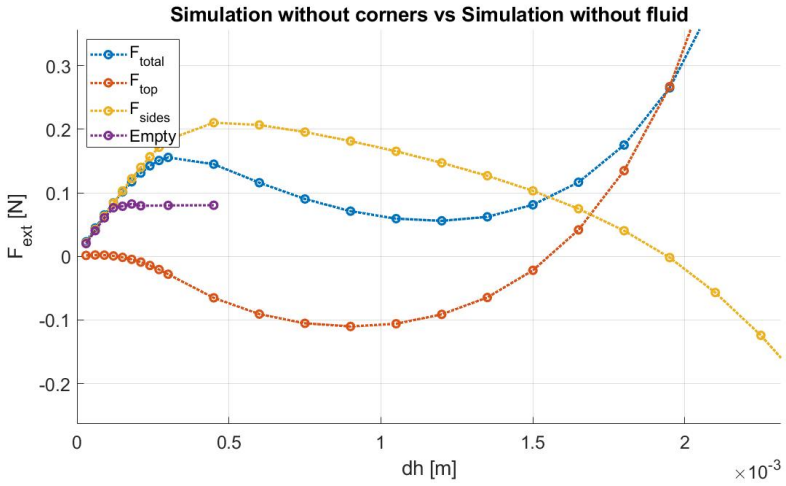

Figure 5.4: Reaction forces defined in Fig. 4.1 for the simulation without corners and reaction solution (same as Fig. 5.3 zoomed in) of simulation without fluid

5.3 Simulation vs Analysis Axial Compression

The purple line in the Fig. 5.5 is the deformation of a beam under axial compression (Eq. 4.1). The simulation without the fluid (yellow) results in the same trend as deformation of the beam under axial loading (purple) until the critical load (P_{crit}=0.0732 N). The simulation with the fluid (red) has the same slope and seams to have a higher critical load. The analysis curve (Eq. 3.22) with α=0.05 has the same trend but deviates for a smaller force. α =0.05 is chosen because in the simulation below the critical load forces on the top are approximately 5% of the sides (Fig. 5.3).

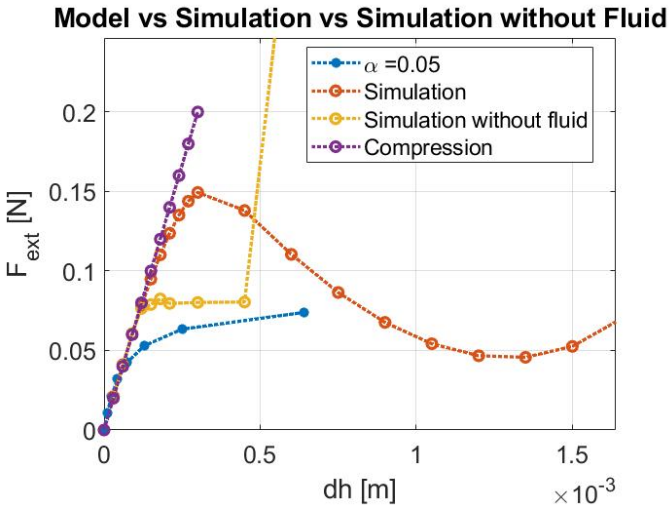

Figure 5.5: External force against relative small displacements where blue line is Eq. 3.22, red line is simulation, yellow is simulation without fluid and purple is Eq. 4.1

5.4 Simulation vs Analysis Axial Tension

In Fig. 5.6 the results are shown for 1mm and 2mm thickness and are compared with the analysis of Eq. 3.22 with α between 1 and 2. The values for α are chosen such that they more or less fit.

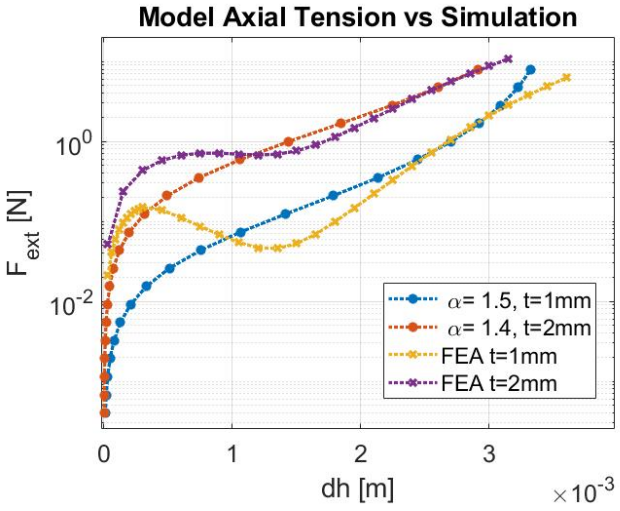

Figure 5.6: External force against displacement for simulation and analysis axial tension of Eq. 3.22 for 1 mm and 2 mm thickness

Concluding this chapter, the structure in the finite element analysis (FEA) results is not stable for limited strains (i.e. buckles). The analysis for with only transverse loading do not approxi-

mate the FEA sufficient. For the small strain the structure stiffness is linear. For larger strains axial loading is negative to approximate the FEA.

6 Discussion

For the first part of the loading of the structure according to the simulation the axial compression Eq. 4.1 is applicable. The range for which this applies is larger than the critical load of the columns. The range of validity is in fact doubled. This implies that the effective stiffness of the structure for strains up to twice the critical force is:

$$E_{\text{struct}} = \frac{2tE}{LH} \tag{6.1}$$

This is a linear stress strain relation which can be favorable for measuring the stiffness of human tissue. For the dimensions shown in Tab. 4.1 this linear stiffness is applicable for up to 1% of the strain of the structure, see Fig. 5.5. For thicker side walls of the structure the critical force is higher (see Fig. 5.1) and therefore the regime for which this linear approximation hold is larger. In this case up to 2% strain of the structure.

The reason that this regime seams to be extended is caused by the presence of the water. The presence of water ensures that the area inside the container is constant. For displacements dh higher than the critical force the sides want to collapse but they can not because the top and bottom have limited displacements.

The assumption on the boundary conditions (angle with y axis is zero) is valid until 6% strain according to the this simulation (Fig. 5.3). The corner starts have a torsional stiffness for this value which is notable. This can be explained because for small percentages of strain of the structure the forces acting on the walls in mainly axial forces. As soon as the pressure of the fluid is the main force acting on the walls the corner starts bending, resulting in a more compliant structure.

For larger strain of the structure the force as determined by the simulation increases faster than what the analytical model with only lateral load predicts. It looks like the side beams, when loaded beyond the critical force, are under tension instead of compression. The force increases rapidly because tensions on the beams makes the beams stiffer for lateral forces.

The axial force P is negative for larger strains, but this is not caused by the partly negative load, but by elongation of the beams. The deflection of the beam and it associate shortening are not sufficient to 'host' the volume of the displaced fluid. And this results in a negative axial force P. The relation between the elongation of the beam and the axial stress is:

$$H' = \int_0^{H-dh} \sqrt{1+\left(\frac{du}{dy}\right)^2}\, dy \tag{6.2}$$

$$\frac{H'-H}{H} = \frac{P}{tE} \tag{6.3}$$

where H' is the length along the center curve of the beam (the arc length). From the last equation one could calculate P and insert it again in Eq. 3.17. This lead to some kind of reiterative calculation because the length H' can not be calculated without a deflection of the beam u.

A negative axial force as modeled in section 3.3 might takes into account the result of axial tension. But not the cause. But the results of this model (blue and red) presented in Fig. 5.6 approximate the simulation (yellow and purple) for section after the dip, i.e. where the negative axial force is acting.

Concluding the discussion, the balance between the lateral load and axial load is changing over displacements. Until the buckling point there is mostly an axial compressing load, then the fluid starts pulling and keep area equal and at a certain displacement the axial force changes sign and is pulling on the boundary.

7 Conclusion

7.1 Conclusion

A fluid filled deformable structure between an ultrasound probe and tissue can be modeled for small strains of the structure as linear. For small strains the thickness of the walls, height, length of the structure and young's modulus of material used characterise the effective stiffness. For larger strains model of the stiffness of the container should also include a negative axial force. Which should be caused by elongation of the beams.

7.2 Recommendations

Besides finding the optimal acoustic impedance match and sensitivity for detection of lesions of the system further research can be done on the topic of total stiffness the structure.

Firstly by finding a proper way to take into account the elongation of the beams. The beams are stretching at some point. So far only numerical iterative approximation are possible.

Secondly the model can be extend to a 3 dimensional problem. Where the sides are finite plates instead of infinite long plates

Lastly other geometries could be investigated. For now only a box shaped structure is considered. Maybe cylindrical type of geometries could be interesting.

A Appendix 1

A.1 Integration Constants P =0

$$EIu = -\frac{1}{24}p_0 y^4 + \frac{1}{6}C_1 y^3 + \frac{1}{2}C_2 y^2 + C_3 y + C_4 \tag{A.1}$$

At $y = 0$ the displacement in x direction should be zero $u = 0$

$$0 = -\frac{1}{24}p_0 0^4 + \frac{1}{6}C_1 0^3 + \frac{1}{2}C_2 0^2 + C_3 0 + C_4$$
$$C_4 = 0$$

At $y = 0$ the angle should be zero $\theta = \frac{du}{dy} = 0$

$$0 = -\frac{1}{6}p_0 0^3 + \frac{1}{2}C_1 0^2 + C_2 0 + C_3$$
$$C_3 = 0$$

At $y = H - dh$ the angle should be zero $\theta = \frac{du}{dy} = 0$

$$0 = -\frac{1}{6}p_0 (H-dh)^3 + \frac{1}{2}C_1 (H-dh)^2 + C_2 (H-dh)$$
$$C_2 = \frac{1}{6}p_0 (H-dh)^2 - \frac{1}{2}C_1 (H-dh)$$
$$C_2 = -\frac{p_0}{12}(H-dh)$$

At $y = H - dh$ the displacement in x direction should be zero $u = 0$

$$0 = -\frac{1}{24}p_0 (H-dh)^4 + \frac{1}{6}C_1 (H-dh)^3 + \frac{1}{2}C_2 (H-dh)^2$$
$$0 = -\frac{1}{24}p_0 (H-dh)^4 + \frac{1}{6}C_1 (H-dh)^3 + \frac{1}{2}\left(\frac{1}{6}p_0 (H-dh)^2 - \frac{1}{2}C_1 (H-dh)\right)(H-dh)^2$$
$$C_1 = \frac{p_0}{2}(H-dh)$$

A.2 Integration Constants P $\neq 0$

$$u(y) = C_1 \sin(ky) + C_2 \cos(ky) + C_3 y + C_4 + \frac{qy^2}{2P} \tag{A.6}$$

At $y = 0$ the angle should be zero $\theta = \frac{du}{dy} = 0$.

$$C_1 k + C_3 = 0$$

At $y = H - dh$ the angle should be zero $\theta = \frac{du}{dy} = 0$.

$$C_1 k \cos(k(H-dh)) - C_2 k \sin(k(H-dh)) + C_3 + \frac{q(H-dh)}{P} = 0$$

Combining these two:

$$-C_3\cos(k(H-dh)) - C_2 k\sin(k(H-dh)) + C_3 + \frac{q(H-dh)}{P} = 0$$
$$C_3\,(1-\cos k(H-dh)) = C_2 k\sin k(H-dh) - \frac{q(H-dh)}{P}$$
$$C_3 = \frac{C_2 kP\sin(k(H-dh)) - q(H-dh)}{P\{1-\cos(k(H-dh))\}}$$

At $y = H - dh$ the deflection should be zero $u = 0$.

$$C_1\cos(k(H-dh)) + C_2\sin(k(H-dh)) + C_3(H-dh) + C_4 + \frac{q(H-dh)^2}{2P} = 0$$

At $y = 0$ the deflection should be zero $u = 0$.

$$C_2 + C_4 = 0$$

Combining above equations.

$$\frac{C_3}{k}\sin(k(H-dh)) + C_2\cos(k(H-dh)) + C_3(H-dh) - C_2 + \frac{q(H-dh)^2}{2P} = 0$$

$$\frac{C_2 kP\sin(k(H-dh)) - q(H-dh)}{Pk\{1-\cos(k(H-dh))\}}\sin(k(H-dh)) + C_2\cos(k(H-dh)) + C_3(H-dh) - C_2 + \frac{q(H-dh)^2}{2P} = 0$$

$$C_2\left(\frac{-\sin^2(k(H-dh))}{1-\cos(k(H-dh))} + \cos(k(H-dh)) + \frac{k(H-dh)\sin(k(H-dh))}{1-\cos(k(H-dh))} - 1\right) =$$
$$-\frac{q(H-dh)\sin(k(H-dh))}{kP(1-\cos(k(H-dh)))} + \frac{q(H-dh)^2}{2P(1-\cos(k(H-dh)))} - \frac{q(H-dh)^2}{2P}$$

$$C_2 = \frac{-2q(H-dh)\sin(k(H-dh)) + 2q(H-dh)^2 k - q(H-dh)^2 k(1-\cos(k(H-dh)))}{2Pk(1-\cos(k(H-dh)))}$$
$$\cdot\frac{(1-\cos(k(H-dh)))}{-\sin^2(k(H-dh)) + \cos(k(H-dh) - \cos^2(k(H-dh))) + k(H-dh)\sin(k(H-dh)) - \cos(k(H-dh))}$$

$$C_2 = \frac{2q(H-dh)\sin(k(H-dh)) + 2q(H-dh)^2 k - q(H-dh)^2 k\{1-\cos(k(H-dh))\}}{2Pk\{2\cos(k(H-dh)) + k(H-dh)\sin(k(H-dh)) - 2\}}$$

B Appendix 2

```
!Nart Pistorius
! Get in the begin level, clear the databse
! and go to the preprocessor
finish
/clear
/prep7
! Define Dimensions as parameters
/units,SI
dpth = 1E-3
wdth = 7E-2
hght = 3E-2
thk = 1E-3
! Build two rectangles and subtract the inner one
!  to make an enclosure
block,-1*wdth/2,wdth/2,-1*hght/2,hght/2,-1*dpth/2,dpth/2 ! outer rectangle area
block,-1*wdth/2+thk,wdth/2-thk,-1*hght/2+thk,hght/2-thk,-1*dpth/2,dpth/2
! inner rectangle area
vsbv,1,2 ! subtracts volumes from volumes
! Make a component out of the inner lines - this is
!  where we will put our HDSP elements
asel,s,areas,,7,12 ! select a subset of area Vmin Vmax
cm,A_insd,areas ! Groups geometry items into a component

asel,s,area,,3,3
cm,bottom,area

asel,s,area,,4,4
cm,top,area

asel,s,area,,13
cm,side_ar,area

! Define a 182 for the solid and 241 for the fluid
et,1,185 ! defines a local element type from library
et,2,HSFLD242
keyopt,2,6,1
keyopt,2,1,0

! Sort of soft material for the enclosure wall
mp,ex,1,0.01e6 ! linear material property
mp,nuxy,1,.49
mp,dens,1,.001

! Some fluid properties
tb,fluid,2,,,,liquid   ! Liquid Properties
tbdata,1,300000        ! Bulk Modulous
tbdata,2,6.4e-4        ! Coeficient of thermal exp.
tbdata,3,.001          ! Density
```

```
FLST,2,4,5,ORDE,2
FITEM,2,9
FITEM,2,-12
AADD,P51X
ESIZE,2e-4,0,
CM,_Y,VOLU
VSEL, , , ,3
CM,_Y1,VOLU
CHKMSH,'VOLU'
CMSEL,S,_Y
!*
VSWEEP,_Y1
!*
CMDELE,_Y
CMDELE,_Y1
CMDELE,_Y2


! Grab the inside nodes from the compenent and create
!   the fluid mesh using esurf
cmsel,s,A_insd ! select
nsla,s,1 ! secect notes from selected area
type,2 ! sets the elements type attribute pointer
mat,2 ! Sets the element material attribute pointer.
n,999999,0,0 ! defines a node
esurf,999999   ! Tell esurf to make the "extra" node 999
allsel,all


! Fix the bottom of the enclosure vertically
!  And fix the bottom right corner tangentially
!  to constrain the model
cmsel,s,top
nsla,s,1 ! select subset of nodes
d,all,uy ! defines DOF constrain uy
d,all,ux
d,all,uz

cmsel,s,side_ar
nsla,s,1
d,all,uz

cmsel,s,bottom,
nsla,s,1
d,all,uy,15*hght/100
d,all,uz ! defines DOF constrain uy
d,all,ux

!allsel,all
!d,999999,hdsp
```

```
allsel,all

/solu
antype,0
NLGEOM,on
NSUBST,20,30,1
AUTOTS,1
TIME,200
CNVTOL,F, ,0.01,2, ,
CNVTOL,U, ,0.01,2, ,

solve
finish
/post1
/DSCALE,ALL,1.0

cmsel,s,bottom,
nsla,s,1
PRRSOL,FY
```

C Appendix 3

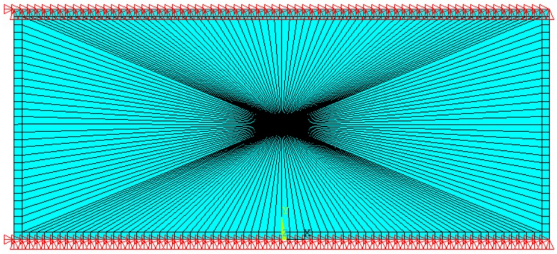

Figure C.1: Boundary conditions with a large mesh size for the illustration. The top and bottom nodes are fixed in x- and y-direction

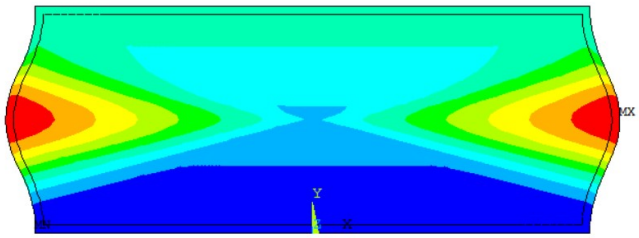

Figure C.2: Displacement vector for $dh = 5\%$ of the height

Bibliography

ANSYS, Inc. (2020), ANSYS 2020 APDL.
https://www.ansys.com/academic

Baranowski, P., R. Gieleta, J. Małachowski and Ł. Mazurkiewicz (2013), Rubber structure under dynamic loading–computational studies, **vol. 61**, no.1, pp. 33–46.

Beer, F. P. (2012), *Mechanics of Materials*, McGraw-Hill.

Burcher, M. R., J. A. Noble, L. Man and M. Gooding (2005), A system for simultaneously measuring contact force, ultrasound, and position information for use in force-based correction of freehand scanning, **vol. 52**, no.8, pp. 1330–1342.

Garett, S. L. (2017), *Understanding Acoustics*, Springer, Cham.

Krouskop, T., T. Wheeler, F. Kallel, B. Garra and T. Hall (1998), The Elastic Moduli of Breast and Prostate Tissues Under Compression, *Ultrasonic imaging*, **vol. 20**, pp. 260–74, doi:10.1177/016173469802000403.

Siemens (2004), ACUSON P500™ Ultrasound System.
siemens-acuson-p500-release-2.0-transducers.pdf

Timoshenko, Stephen P., G. J. M. (1989), Dover Publications, ISBN 978-0-486-47207-2.
https://app.knovel.com/hotlink/toc/id:kpTESE0003/theory-elastic-stability/theory-elastic-stability

Tzias, D. D., E. A. O'Flynn, S. D. Allen and R. M. Wilson (2018), *Current Status and New Developments in Breast Cancer Diagnosis and Detection*, European Oncology Haematology.
http://doi.org/10.17925/EOH.2013.09.1.21

Wauben, B. (2018), *Borstkanker*.
https://www.kanker.nl/kankersoorten/borstkanker/algemeen/overlevingscijfers-borstkanker

Wolbarst, A. (1993), *Physics of Radiology*, Appleton Lange, Norwar.

Zhang, Y. (2013), Measuring Acoustic Attenuation of Polymer Materials Using Drop Ball Test, *Dissertations and Theses*.